

AN IRON K COMPONENT TO THE ULTRAFAST OUTFLOW IN NGC 1313 X-1

D. J. WALTON^{1,2}, M. J. MIDDLETON³, C. PINTO³, A. C. FABIAN³, M. BACHETTI⁴, D. BARRET^{5,6}, M. BRIGHTMAN², F. FUERST²,
F. A. HARRISON², J. M. MILLER⁷, D. STERN¹,

¹ Jet Propulsion Laboratory, California Institute of Technology, Pasadena, CA 91109, USA

² Space Radiation Laboratory, California Institute of Technology, Pasadena, CA 91125, USA

³ Institute of Astronomy, University of Cambridge, Madingley Road, Cambridge CB3 0HA, UK

⁴ INAF/Osservatorio Astronomico di Cagliari, via della Scienza 5, I-09047 Selargius (CA), Italy

⁵ Universite de Toulouse; UPS-OMP; IRAP; Toulouse, France

⁶ CNRS; IRAP; 9 Av. colonel Roche, BP 44346, F-31028 Toulouse cedex 4, France

⁷ Department of Astronomy, University of Michigan, 1085 S. University Ave., Ann Arbor, MI, 49109-1107, USA

Draft version August 27, 2018

ABSTRACT

We present the detection of an absorption feature at $E = 8.77_{-0.06}^{+0.05}$ keV in the combined X-ray spectrum of the ultraluminous X-ray source NGC 1313 X-1 observed with *XMM-Newton* and *NuSTAR*, significant at the 3σ level. If associated with blueshifted ionized iron, the implied outflow velocity is $\sim 0.2c$ for Fe XXVI, or $\sim 0.25c$ for Fe XXV. These velocities are similar to the ultrafast outflow seen in absorption recently discovered in this source at lower energies by *XMM-Newton*, and we therefore conclude that this is an iron component to the same outflow. Photoionization modeling marginally prefers the Fe XXV solution, but in either case the outflow properties appear to be extreme, potentially supporting a super-Eddington hypothesis for NGC 1313 X-1.

Subject headings: Black hole physics – X-rays: binaries – X-rays: individual (NGC 1313 X-1)

1. INTRODUCTION

Ultraluminous X-ray sources (ULXs) are variable, off-nuclear point sources in nearby galaxies with X-ray luminosities $L_X \geq 10^{39}$ erg s⁻¹ (Swartz et al. 2004; Walton et al. 2011). The brighter members of this population have luminosities that significantly (factors of 10 or more) exceed the Eddington limit for the $\sim 10 M_\odot$ stellar-remnant black holes observed in accreting Galactic black hole binaries (Casares & Jonker 2014). Multi-wavelength observations have largely ruled-out strong anisotropic emission as a means of skewing luminosity estimates (Moon et al. 2011, although moderate collimation is still permitted). ULXs must therefore either host large black holes, potentially either the long-postulated yet elusive ‘intermediate mass’ black holes ($M_{\text{BH}} \sim 10^2\text{--}5 M_\odot$; Miller et al. 2004) or the massive stellar remnants ($M_{\text{BH}} \sim 30\text{--}100 M_\odot$; Zampieri & Roberts 2009) recently confirmed by LIGO (Abbott et al. 2016), or represent an exotic, highly super-Eddington accretion phase (Poutanen et al. 2007). In either case, they hold clues to the processes governing the formation and evolution of super-massive black holes in the early Universe (Kormendy & Ho 2013).

Since launch, the *NuSTAR* mission (Harrison et al. 2013) has undertaken a substantial program observing a sample of extreme ULXs, revealing the high-energy ($E > 10$ keV) behavior of these enigmatic sources for the first time. As one of the few sources within ~ 5 Mpc to persistently radiate at $L_X \sim 10^{40}$ erg s⁻¹ (Miller et al. 2013), NGC 1313 X-1 ($D \sim 4$ Mpc) was an important part of this program, observed in coordination with *XMM-Newton* (Jansen et al. 2001) to provide broadband ($\sim 0.3\text{--}30$ keV) spectral coverage. These observations revealed broadband spectra inconsistent with standard modes of sub-Eddington accretion (Bachetti et al. 2013; Miller et al. 2014; similar to other ULXs observed by *NuSTAR* to date, Walton et al. 2014, 2015a,b; Rana et al. 2015; Mukherjee et al. 2015), supporting the idea that these sources

are exhibiting a super-Eddington phase of accretion. Indeed, we now know at least one of these sources is a highly super-Eddington neutron star (Bachetti et al. 2014).

A prediction of all super-Eddington accretion models is that powerful winds should be launched (Poutanen et al. 2007; King 2009; Dotan & Shaviv 2011; Takeuchi et al. 2013). Robust detection of any such winds from ULXs has, however, proven challenging (Walton et al. 2012, 2013). For NGC 1313 X-1, Middleton et al. (2015b) report low-energy (~ 1 keV) blended atomic features that are consistent with being absorption from an ionised outflow, but the low-resolution CCD spectra considered prevented a conclusive identification as such. However, in a key breakthrough, a recent follow-up analysis by Pinto et al. (2016) utilizing the high-resolution reflection grating spectrometer (RGS) aboard *XMM-Newton* was able to resolve this low-energy spectral structure into several discrete emission and absorption features, and found that NGC 1313 X-1 does indeed exhibit an extreme ionised outflow, potentially consisting of multiple velocity components spanning $\sim 0.2\text{--}0.25c$.

Here, by considering the high-energy *XMM-Newton* and *NuSTAR* data available for NGC 1313 X-1, we report on a detection of an ionized iron K α component to the ultrafast outflow (UFO) discovered by Pinto et al. (2016).

2. OBSERVATIONS AND DATA REDUCTION

NGC 1313 X-1 has frequently been observed in the X-ray band and is known to be a variable source, exhibiting high- and low-states with significantly different spectra (Feng & Kaaret 2006; Pintore & Zampieri 2012; Middleton et al. 2015a, Bachetti et al. in preparation). The majority of the X-ray observations in the archive cover the low-flux state, so we focus on these data in order to maximise the integrated signal-to-noise (S/N) in the iron K bandpass while considering only observations with similar spectra. *XMM-Newton*, in particular, has frequently observed NGC 1313, but many of these observations are short and

have X-1 placed off-axis. The EPIC-pn detector aboard *XMM-Newton* is known to have increased background emission from copper lines at ~ 8 keV away from the optical axis (Carter & Read 2007), which fall in the energy range of interest for any iron line searches given the velocities reported by Pinto et al. (2016). We therefore also limit our analysis to *XMM-Newton* observations where NGC 1313 X-1 was the primary target. In total, we consider the three full-orbit *XMM-Newton* observations (OBSIDs 0405090101, 0693850501, 0693851201; note that these are the same *XMM-Newton* observations considered by Pinto et al. 2016), and the two long *NuSTAR* observations presented in Bachetti et al. (2013, OBSIDs 30002035002 and 30002035004).

The data from these observations are reduced individually, and then combined into a set of average spectra using ADDASCASPEC. In all cases, source products are extracted from a circular region of radius $40''$ since there is another X-ray source $\sim 55''$ to the south (Bachetti et al. 2013). This aperture gave the best balance between maximising the S/N for X-1 and minimising contamination from this other source. Background is always estimated from significantly larger regions of blank sky on the same detector as X-1 to ensure it is well sampled. Finally, each of the average spectra are rebinned to a minimum of 25 counts per bin to allow the use of χ^2 minimization during spectral fitting. The following sections provide further technical details regarding our reduction of these data.

2.1. *NuSTAR*

The *NuSTAR* data were reduced using the standard pipeline, NUPIPELINE, part of the *NuSTAR* Data Analysis Software (v1.4.1). *NuSTAR* caldb v20150316 is used throughout. The unfiltered event files were cleaned with the standard depth correction, significantly reducing the internal background, and passages through the South Atlantic Anomaly were removed. Source spectra and instrumental responses were produced for both of the focal plane modules (FPMA/B) using NUPRODUCTS. In addition to the standard ‘science’ data, we also extract the ‘spacecraft science’ data following Walton et al. (2016), which in this case provides $\sim 35\%$ of the total 360 ks (per FPM) good exposure.

2.2. *XMM-Newton*

The *XMM-Newton* data were reduced with the *XMM-Newton* Science Analysis System (v14.0.0), following the standard prescription.¹ Raw data files were cleaned using EPCCHAIN for EPIC-pn (Strüder et al. 2001), and EMCHAIN for the EPIC-MOS detectors (Turner et al. 2001). Only single–double (PATTERN ≤ 4) and single–quadruple (PATTERN ≤ 12) events were considered for EPIC-pn and EPIC-MOS, respectively. Periods of high background were excluded, as were events close to edge/bad pixels (FLAG=0). Instrumental response files were generated with RMFGEN and ARFGEN, and the data from the two EPIC-MOS detectors were combined together. The total good exposure is 258 ks for EPIC-pn, and 331 ks for each EPIC-MOS unit.

3. SPECTRAL ANALYSIS

Our goal in this work is to search for any ionized iron $K\alpha$ absorption features in the X-ray spectrum of NGC 1313 X-1 that might be associated with the UFO discovered by

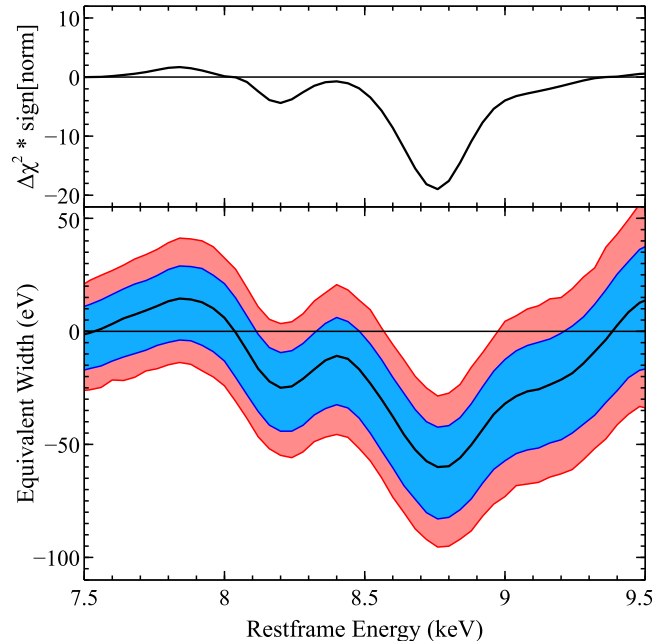


FIG. 1.— A zoom in on the line-search results for the absorption feature detected in our analysis. Top: the $\Delta\chi^2$ improvement obtained with the addition of a narrow Gaussian line, as a function of line energy, for NGC 1313 X-1. Positive values indicate the best fit line is in emission, and negative values indicate absorption. The feature at ~ 8.8 keV gives an improvement of $\Delta\chi^2 = 19.5$. Bottom: 90% (blue) and 99% (red) confidence contours for the equivalent width of the narrow line included. We find this feature at ~ 8.8 keV to have $\text{EW} = 61 \pm 24$ eV. No other significant features are detected.

Pinto et al. (2016). We use XSPEC v12.8.2 (Arnaud 1996) for our spectral analysis, and unless stated otherwise parameter uncertainties are quoted at 90% confidence for one parameter of interest. Our data selection is such that we can apply a common model to all the datasets, accounting for differences in the average *XMM-Newton* and *NuSTAR* fluxes and residual cross-calibration uncertainties between the detectors by allowing multiplicative constants to float between them, fixing EPIC-pn to unity. The EPIC-pn and EPIC-MOS detectors agree to within 5%, as do FPMB and FPMB, while the average *XMM-Newton* and *NuSTAR* fluxes resulting from our data selection only differ by $\sim 10\%$, which is broadly similar to the absolute cross-calibration differences seen between the two missions (Madsen et al. 2015).

We begin by constructing a simple model for the continuum. In this work, we focus on the 3–20 keV bandpass, providing sufficient coverage to accurately model the continuum local to the iron band with a simple model, while remaining independent of the low-energy X-ray band in which the outflow was initially discovered. The spectral curvature seen from NGC 1313 X-1 over this energy range is well established (Stobbart et al. 2006; Gladstone et al. 2009; Bachetti et al. 2013), so we model the continuum as a cutoff powerlaw. We also include neutral absorption, both from our Galaxy ($N_{\text{H,Gal}} = 4.1 \times 10^{20} \text{ cm}^{-2}$; Kalberla et al. 2005) and intrinsic to NGC 1313 ($z = 0.00157$). However, given the limited bandpass considered, we are not particularly sensitive to the level of absorption seen towards NGC 1313 X-1, so we fix the intrinsic column to $N_{\text{H,int}} = 2.7 \times 10^{21} \text{ cm}^{-2}$ (Miller et al. 2013). These neutral absorption components are modeled with TBABS, adopting the abundance set of Wilms et al. (2000) and cross-sections of Verner et al. (1996).

¹ <http://xmm.esac.esa.int/>

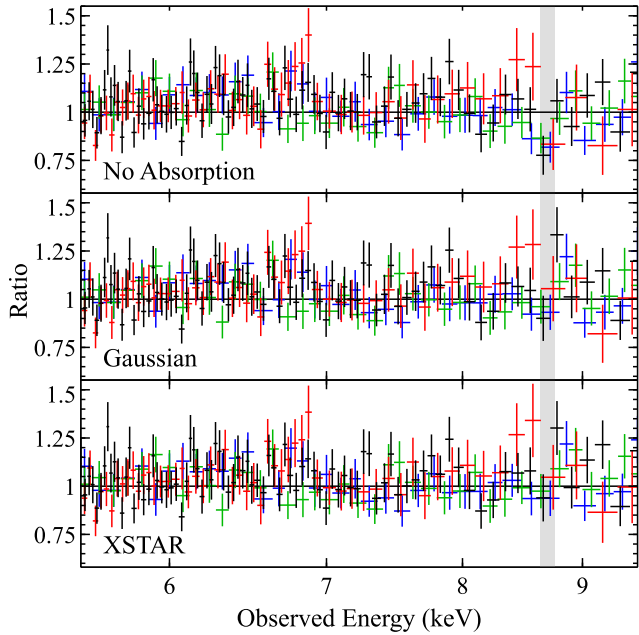


FIG. 2.— Data/model ratio plots for our basic continuum model (*top panel*), the model including a Gaussian absorption line (*middle panel*) and the model including a physical photoionised absorber (XSTAR; *bottom panel*). Data from EPIC-pn, EPIC-MOS, FPMA and FPMB are shown in black, red, green and blue, respectively. The feature at ~ 8.8 keV is indicated with the grey shaded region; all of the detectors used in this work show low residuals at the same energy, which are improved in the models including a Gaussian and an XSTAR absorption component.

This provides an excellent fit to the 3–20 keV emission, with $\chi^2/\text{degrees of freedom} = 1634/1627$. The photon index and high-energy cutoff obtained are $\Gamma = 0.96 \pm 0.07$ and $E_{\text{cut}} = 5.5^{+0.4}_{-0.3}$ keV, and the model normalisation is $(4.0 \pm 0.2) \times 10^{-4}$ ct keV $^{-1}$ cm $^{-2}$ s $^{-1}$ (at 1 keV).

To search for atomic features, we follow a similar approach to Walton et al. (2012, 2013). We refer the reader to those works for a detailed description, but in brief, we include a narrow (intrinsic width of $\sigma = 10$ eV) Gaussian, and vary its energy across the energy range of interest in steps of 40 eV (oversampling the *XMM-Newton* energy resolution by a factor ~ 4 –5). The Gaussian normalisation can be either positive or negative. For each line energy, we record the $\Delta\chi^2$ improvement in fit resulting from the inclusion of the Gaussian line, as well as the best fit equivalent width (*EW*) and its 90 and 99% confidence limits. These are calculated with the EQWIDTH command in XSPEC, using 10,000 parameter simulations based on the best fit model parameters and their uncertainties. To be conservative, we vary the Gaussian line energy between 6.6 and 9.6 keV, corresponding to a wide range of outflow velocities extending up to $>0.25c$ for Fe XXVI.

The results are shown in Figure 1. We find the addition of a Gaussian absorption line at ~ 8.8 keV provides a notable improvement to the fit. Allowing the line parameters to vary freely, we find a line energy of $E = 8.77^{+0.05}_{-0.06}$ keV, an equivalent width of $EW = -61 \pm 24$ eV (comparable to the strongest iron absorption seen from a black hole binary to date; King et al. 2012). This gives an improvement to the fit of $\Delta\chi^2 = 19.5$ for three extra free parameters. The line is consistent with being unresolved at the resolution of the *XMM-Newton* and *NuSTAR* detectors ($\sigma < 0.24$ keV). Assuming an association with iron, the extreme energy of this

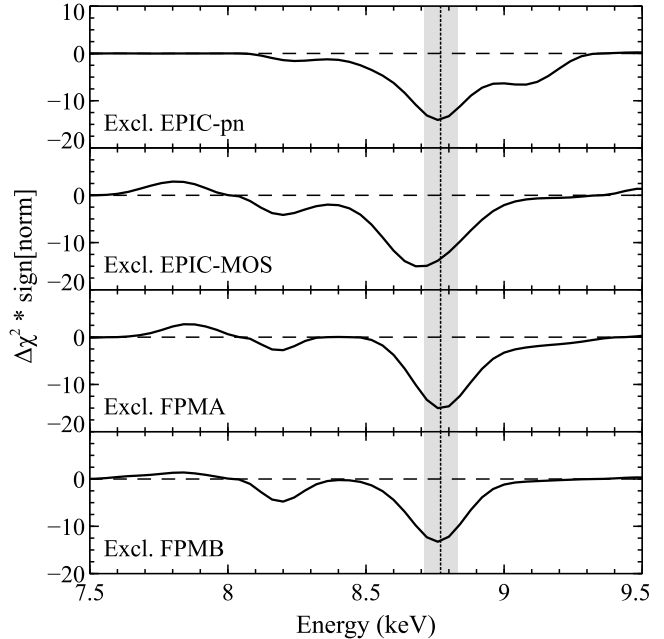


FIG. 3.— The results obtained repeating our line-search analysis after excluding each of the detectors utilized in turn. In all cases, the same feature is picked out. The significance is lower, as expected given the loss of S/N, but the improvement is still always $\Delta\chi^2 = 13 - 15$ (for 3 extra DoF). The dotted line and grey shaded region indicate the best-fit line energy and its uncertainty from the full analysis incorporating all detectors.

feature makes an association with either Fe XXV or Fe XXVI K α (6.67 and 6.97 keV, respectively) the most likely. This would imply an outflow velocity of $\sim 0.2c$ for Fe XXVI, or an even more extreme velocity of $\sim 0.25c$ for Fe XXV. No other features provide such a strong improvement in the fit.

In Figure 2 we show the data/model ratios for the model excluding and including this absorption line. The feature is not particularly visually prominent, and would be lost in the noise for any of the detectors individually. However, the key to the statistical improvement observed is that all of the detectors show low residuals to the continuum model at the same energy. In Figure 3 we show the same line search applied excluding each of the four detectors utilized in this work in turn. In each of these cases, the improvement provided by including an absorption line at ~ 8.8 keV is still $\Delta\chi^2 = 13 - 15$. This strongly implies that this feature cannot be related to systematic effects (*e.g.* instrumental background), which differ for each of these detectors.

3.1. Significance Simulations

In order to assess the statistical significance of this potential Fe K absorption feature, we performed a series of spectral simulations. Using the same response and background files, and adopting the same exposure times as the real data used here, we simulated 10,000 sets of *XMM-Newton* (pn, combined MOS1 and MOS2) and *NuSTAR* (FPMA, FPMB) spectra with the FAKEIT command in XSPEC based on the best-fit cutoff powerlaw continuum (*i.e.* without any absorption feature included). Each of the simulated datasets was rebinned in the same manner and analysed over the same bandpass as adopted for the real data. We then fit each of the combined datasets with a cutoff powerlaw continuum, and subsequently applied an identical line search as performed above (thus the number of energy bins searched is fully accounted for). Of the 10,000 datasets simulated, only 31 returned a chance im-

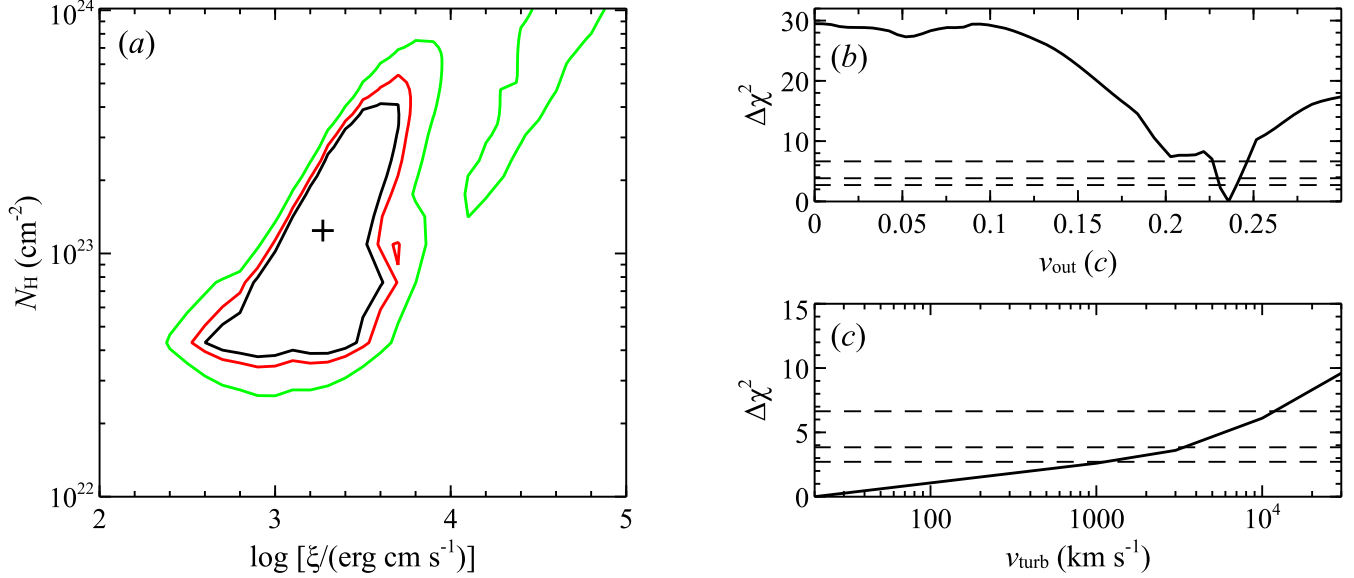


FIG. 4.— Confidence contours for the column density and ionisation parameter (2D; panel *a*), the outflow velocity (panel *b*), and the turbulent velocity broadening (panel *c*) obtained from our photoionisation modeling with XSTAR. Panel *a* shows the 90, 95 and 99% contours for two parameters of interest, and the dashed lines in panels *b* and *c* show these same confidence levels for a single parameter.

provement equivalent to or greater than that observed (at any energy searched), implying that the feature seen in the real data is significant at the $\sim 3\sigma$ level. This is something of a conservative estimate; if we also require that the simulations match the exclusion trial results given above (such that the deviation is not dominated by a single detector), only 12 match the observed characteristics by chance, indicating a $\sim 99.9\%$ detection significance. Using the velocity information from Pinto et al. (2016) as a prior would also serve to further increase the detection significance.

3.2. XSTAR Modeling

We model this absorption feature using a physical model for absorption by a photoionised plasma. Following Middleton et al. (2014), we construct a set of custom photoionized absorption models with XSTAR (Kallman & Bautista 2001), using the continuum emission observed from NGC 1313 X-1 (described above) as the input ionizing continuum. These grids are calculated assuming solar abundances, an ionizing luminosity of 10^{40} erg s^{-1} (typical for NGC 1313 X-1), and a density of 10^{17} cm^{-3} (see Middleton et al. 2014). Free parameters are the ionisation parameter ($\xi = L_{\text{ion}}/nR^2$, where L_{ion} is the ionizing luminosity between 1–1000 Ry, n is the density of the plasma and R is its distance from the ionizing source; ξ is calculated in units of erg $cm s^{-1}$ throughout this work), the column density ($N_{\text{H,ion}}$) and the line-of-sight outflow velocity (v_{out}) of the absorbing medium. We also consider a range of turbulent velocity broadening, v_{turb} , from 20–30,000 $km s^{-1}$, for consistency with Pinto et al. (2016).

The addition of XSTAR to our continuum model provides a more substantial improvement to the fit than the single Gaussian feature: $\Delta\chi^2 = 29$ for three extra free parameters. This may suggest that, in addition to the feature at ~ 8.8 keV, there are further weak features in the spectrum that are associated with the same outflow but not significantly detected individually. We find $\log \xi = 3.3^{+0.3}_{-0.5}$, $N_{\text{H,ion}} = (1.2^{+2.1}_{-0.8}) \times 10^{23}$ cm^{-2} , $v_{\text{out}} = 0.236 \pm 0.005c$,

and $v_{\text{turb}} < 1000$ $km s^{-1}$. Although $\log \xi \sim 3.3$ is preferred, there is a degeneracy between the ionisation parameter and the column density (Figure 4). This is not surprising given that the observational signature of this absorber is dominated by a single line, making it difficult to distinguish between ionisation states dominated by Fe XXV ($\log \xi \sim 3.3$) and Fe XXVI ($\log \xi \sim 4.5$; see e.g. King et al. 2014). The velocity contour therefore also shows two minima with similarly good fits (the second being at $v_{\text{out}} \sim 0.2c$; Figure 4), corresponding to these two potential solutions.

4. DISCUSSION AND CONCLUSIONS

We have presented the detection of an absorption feature at $E = 8.77^{+0.05}_{-0.06}$ keV in the X-ray spectrum of the ULX NGC 1313 X-1, found by combining data from the *XMM-Newton* and *NuSTAR* observatories. Owing to the extreme energy of this feature, and the low flux of NGC 1313 X-1, the combination of *XMM-Newton* and *NuSTAR* is particularly vital to this detection. This provides a broad bandpass, enabling robust continuum estimation both above and below the line energy, and significantly enhances the S/N over what each observatory individually would return in commensurate exposure times. Both of these issues hindered our previous attempt to search for absorption in NGC 1313 X-1 (using *XMM-Newton* only; Walton et al. 2012) to the extent that this feature could not be seen. Furthermore, the combination of the different detectors aboard *XMM-Newton* and *NuSTAR* allows us to effectively rule out an instrumental systematic origin, given that all the detectors utilized show consistent low residuals to the continuum emission.

Associating this feature with highly ionised iron, either Fe XXV or Fe XXVI, implies an extreme outflow velocity of 0.2–0.25 c . Photoionisation modeling marginally prefers a solution in which this absorption is dominated by Fe XXV ($\log \xi \sim 3.3$, $v_{\text{out}} \sim 0.25c$), but with the observational signature of this absorber being dominated by this single line there is significant degeneracy, with solutions dominated by Fe XXVI ($\log \xi \sim 4.5$, $v_{\text{out}} \sim 0.2c$) providing similarly good fits. These velocities are consistent with the UFO recently dis-

covered by Pinto et al. (2016), that was identified through the detection of highly blue-shifted absorption lines from moderately ionised material in the low-energy X-ray band, suggesting that we are seeing an iron $K\alpha$ component associated with the same outflow. Ionized iron $K\alpha$ absorption features associated with UFOs ($v_{\text{out}} > 0.1c$) have been seen in several active galaxies (e.g. Tombesi et al. 2010), but never before from an X-ray binary. We note that the energy of the detected feature is just about consistent with the rest-frame energy of the Fe XXV edge at 8.83 keV. However, the data prefer the feature to be narrow, and no corresponding absorption line is seen at 6.67 keV, hence an ionized absorber at rest provides a significantly worse fit in our photoionization modeling ($\Delta\chi^2 \sim 29$).

Pinto et al. (2016) consider two possibilities for the outflow structure: a single zone with low velocity broadening ($v_{\text{turb}} = 20 \text{ km s}^{-1}$), and two zones, the second of which has a much higher broadening ($v_{\text{turb}} = 10,000 \text{ km s}^{-1}$). The line detected here is narrow; broadening at the latter level seems to be unlikely. We therefore compare our results to the former scenario. Although there is significant degeneracy in our results (Figure 4), the absorption detected here is significantly more ionized, and has a significantly larger column; Pinto et al. 2016 found $\log \xi \sim 2.3$, and $N_{\text{H}} \sim 2 \times 10^{22} \text{ cm}^{-2}$ for their one-zone model. The absorption detected here may thus arise in a phase of the outflow located closer to the black hole than that contributing the features detected in the RGS. The contrast between v_{out} and v_{turb} is larger than inferred for the UFOs in PDS456 (Nardini et al. 2015) and PG1211+143 (Pounds et al. 2003), despite the similar Gaussian line width constraints. If real, this may provide some clue to the wind geometry, implying that we might not directly view the primary acceleration region, otherwise a smaller contrast would have been expected. However, the constraint on v_{turb} is ionization dependent, with the higher ionization solution allowing for v_{turb} up to $10,000 \text{ km s}^{-1}$, more comparable with these other cases.

This additional phase of absorption would significantly increase the total mass outflow rate (\dot{M}_{out}) compared to that inferred from just the low-energy absorption alone. Combining the standard expression for \dot{M}_{out} and the definition of the ionisation parameter, we can estimate the kinetic luminosity of the outflow ($L_{\text{kin}} = 1/2\dot{M}v_{\text{out}}^2$) relative to the bolometric radiative luminosity (L_{bol}):

$$\frac{L_{\text{kin}}}{L_{\text{bol}}} \approx 2\pi m_p \mu \frac{L_{\text{ion}}}{L_{\text{bol}}} \frac{v_{\text{out}}^3}{\xi} \Omega C_V \quad (1)$$

where m_p is the proton mass, μ is the mean atomic weight (~ 1.2 for solar abundances), Ω is the (normalized) solid angle subtended by the wind, and C_V is its volume filling factor (or its ‘clumpiness’). Although some extrapolation beyond the observed bandpass is necessary, the broadband continuum models constructed by Bachetti et al. (2013) and Miller et al. (2014) imply $L_{\text{ion}}/L_{\text{bol}} \sim 0.85$. We therefore find $L_{\text{kin}}/L_{\text{bol}} \sim 1500\Omega C_V$ and $\sim 60\Omega C_V$ for the lower and higher ionisation solutions, respectively. Thus unless it either has a very small solid angle or a very low volume filling factor (which may be possible; King et al. 2012), the wind may dominate the energy output from NGC 1313 X-1. While both Ω and C_V are unknown, the above $L_{\text{kin}}/L_{\text{bol}}$ values are extreme in comparison to similar calculations for even the strongest outflows seen from sub-Eddington systems (Blustin et al. 2005; King et al. 2012, 2014; Nardini et al. 2015; Miller et al. 2016). This is consistent with the basic expectation for a super-Eddington accretion scenario (Poutanen et al. 2007; King 2009), as suggested by the unusual broadband X-ray spectrum observed (Bachetti et al. 2013).

ACKNOWLEDGEMENTS

The authors would like to thank the anonymous referee for their extremely timely and positive feedback, which helped improve the final manuscript. MJM acknowledges support from an STFC Ernest Rutherford fellowship, CP and ACF acknowledge support from ERC Advanced Grant 340442, and DB acknowledges financial support from the French Space Agency (CNES). This research has made use of data obtained with *NuSTAR*, a project led by Caltech, funded by NASA and managed by NASA/JPL, and has utilized the NUSTARDAS software package, jointly developed by the ASDC (Italy) and Caltech (USA). This research has also made use of data obtained with *XMM-Newton*, an ESA science mission with instruments and contributions directly funded by ESA Member States.

Facilities: NuSTAR, XMM

REFERENCES

- Abbott B. P., Abbott R., Abbott T. D., et al., 2016, *Physical Review Letters*, 116, 6, 061102
- Arnaud K. A., 1996, in *Astronomical Data Analysis Software and Systems V*, edited by G. H. Jacoby & J. Barnes, vol. 101 of *Astron. Soc. Pac. Conference Series*, Astron. Soc. Pac., San Francisco, 17
- Bachetti M., Harrison F. A., Walton D. J., et al., 2014, *Nat*, 514, 202
- Bachetti M., Rana V., Walton D. J., et al., 2013, *ApJ*, 778, 163
- Blustin A. J., Page M. J., Fuerst S. V., Branduardi-Raymont G., Ashton C. E., 2005, *A&A*, 431, 111
- Carter J. A., Read A. M., 2007, *A&A*, 464, 1155
- Casares J., Jonker P. G., 2014, *Space Sci. Rev.*, 183, 223
- Dotan C., Shaviv N. J., 2011, *MNRAS*, 413, 1623
- Feng H., Kaaret P., 2006, *ApJ*, 650, L75
- Gladstone J. C., Roberts T. P., Done C., 2009, *MNRAS*, 397, 1836
- Harrison F. A., Craig W. W., Christensen F. E., et al., 2013, *ApJ*, 770, 103
- Jansen F., Lumb D., Altieri B., et al., 2001, *A&A*, 365, L1
- Kalberla P. M. W., Burton W. B., Hartmann D., et al., 2005, *A&A*, 440, 775
- Kallman T., Bautista M., 2001, *ApJS*, 133, 221
- King A. L., Miller J. M., Raymond J., et al., 2012, *ApJ*, 746, L20
- King A. L., Walton D. J., Miller J. M., et al., 2014, *ApJ*, 784, L2
- King A. R., 2009, *MNRAS*, 393, L41
- Kormendy J., Ho L. C., 2013, *ARA&A*, 51, 511
- Madsen K. K., Harrison F. A., Markwardt C. B., et al., 2015, *ApJS*, 220, 8
- Middleton M. J., Heil L., Pintore F., Walton D. J., Roberts T. P., 2015a, *MNRAS*, 447, 3243
- Middleton M. J., Walton D. J., Fabian A., et al., 2015b, *MNRAS*, 454, 3134
- Middleton M. J., Walton D. J., Roberts T. P., Heil L., 2014, *MNRAS*, 438, L51
- Miller J. M., Bachetti M., Barret D., et al., 2014, *ApJ*, 785, L7
- Miller J. M., Raymond J., Cackett E., Grinberg V., Nowak M., 2016, *ApJ*, 822, L18
- Miller J. M., Raymond J., Fabian A. C., et al., 2004, *ApJ*, 601, 450
- Miller J. M., Walton D. J., King A. L., et al., 2013, *ApJ*, 776, L36
- Moon D.-S., Harrison F. A., Cenko S. B., Shariff J. A., 2011, *ApJ*, 731, L32
- Mukherjee E. S., Walton D. J., Bachetti M., et al., 2015, *ApJ*, 808, 64
- Nardini E., Reeves J. N., Gofford J., et al., 2015, *Science*, 347, 860
- Pinto C., Middleton M. J., Fabian A. C., 2016, *Nat*, 533, 64
- Pintore F., Zampieri L., 2012, *MNRAS*, 420, 1107
- Pounds K. A., Reeves J. N., King A. R., Page K. L., O’Brien P. T., Turner M. J. L., 2003, *MNRAS*, 345, 705
- Poutanen J., Lipunova G., Fabrika S., Butkevich A. G., Abolmasov P., 2007, *MNRAS*, 377, 1187

- Rana V., Harrison F. A., Bachetti M., et al., 2015, *ApJ*, 799, 121
Stobart A.-M., Roberts T. P., Wilms J., 2006, *MNRAS*, 368, 397
Strüder L., Briel U., Dennerl K., et al., 2001, *A&A*, 365, L18
Swartz D. A., Ghosh K. K., Tennant A. F., Wu K., 2004, *ApJS*, 154, 519
Takeuchi S., Ohsuga K., Mineshige S., 2013, *PASJ*, 65
Tombesi F., Cappi M., Reeves J. N., et al., 2010, *A&A*, 521, A57
Turner M. J. L., Abbey A., Arnaud M., et al., 2001, *A&A*, 365, L27
Verner D. A., Ferland G. J., Korista K. T., Yakovlev D. G., 1996, *ApJ*, 465, 487
Walton D. J., Harrison F. A., Bachetti M., et al., 2015a, *ApJ*, 799, 122
Walton D. J., Harrison F. A., Grefenstette B. W., et al., 2014, *ApJ*, 793, 21
Walton D. J., Middleton M. J., Rana V., et al., 2015b, *ApJ*, 806, 65
Walton D. J., Miller J. M., Harrison F. A., et al., 2013, *ApJ*, 773, L9
Walton D. J., Miller J. M., Reis R. C., Fabian A. C., 2012, *MNRAS*, 426, 473
Walton D. J., Roberts T. P., Mateos S., Heard V., 2011, *MNRAS*, 416, 1844
Walton D. J., Tomsick J. A., Madsen K. K., et al., 2016, *ArXiv* 1605.03966
Wilms J., Allen A., McCray R., 2000, *ApJ*, 542, 914
Zampieri L., Roberts T. P., 2009, *MNRAS*, 400, 677